Available online at www.CivileJournal.org

Civil Engineering Journal

(E-ISSN: 2476-3055; ISSN: 2676-6957)

Vol. 10, No. 02, February, 2024

Behavior of Axially Loaded Concrete Columns Reinforced with Steel Tubes Infilled with Cementitious Grouting Material

Ahlam A. Abbood [1*], Nazar Oukaili [1]

[1] *Department of Civil Engineering, College of Engineering, University of Baghdad, Baghdad 10071, Iraq.*

Received 10 November 2023; Revised 17 January 2024; Accepted 23 January 2024; Published 01 February 2024

Abstract

The paper presents a novel method of reinforcing concrete columns using small-diameter steel tubes instead of traditional steel bars. The researchers conducted experimental investigations on twelve mid-scale circular concrete column specimens, which were divided into two groups consisting of six specimens each: short and long columns. Two of the specimens in each group were reinforced with steel bars, while the remaining four were reinforced with steel tubes filled with cementitious grouting material. The study proposed two concepts for cementitious grouted steel-tube reinforcement. The first concept utilized steel tubes with equivalent net areas to the steel bar areas used in the reference column, while the second concept used steel-tube reinforcement with the same diameter as the steel bars in the reference column. Nonlinear Finite Element (FE) analyses were conducted on experimental specimens using ABAQUS software. The results showed that using steel tubes with an area equivalent to that of steel bars instead of conventional columns increased the bearing capacity of reinforced concrete columns by 17%. Moreover, using steel tubes whose area matched 30% of the steel bar area achieved a bearing capacity of about 81% of the conventional concrete columns. The experimental and FE analysis findings indicate that this methodology can increase the bearing capacity of reinforced concrete columns when compared to traditional methods. The axial load-axial displacement curves, axial load-axial strain curves, and failure load of the FE model all demonstrated good convergence with the experimental data.

Keywords: Composite Column; Concrete Column; Steel Tube; Grouting Material; Spiral Pitch.

1. Introduction

Reinforced concrete RC columns are critical structural elements in buildings. Solid steel bars are traditionally used longitudinally and transversely in concrete column reinforcement. A composite column is used to increase the ductility and bearing capacity of the columns. The economic advantage of composite columns includes providing large load capacity with smaller cross-sectional areas. Especially for high-rise structures, these kinds of columns are mentioned to be widely used. They also achieve higher strength, more stiffness, better protection against fire, and inherent ductility [1–3]. Three methods of composite columns are commonly used in concrete structures, mainly the encased steel-section columns (i.e., the steel section is encased in concrete), the concrete-filled steel tube columns CFST (the exterior steel section is in-filled with concrete), and the encased concrete-filled steel tube columns (the interior steel section is in-filled with concrete and used as a main reinforcement).

In the first method, both the steel and the concrete resist the load by interacting together through friction and chemical bonds. The encased steel-section column offers high strength, good fire resistance, corrosion protection, and significant resistance to lateral loads [4, 5]. Composite columns with structural steel provide improved ultimate axial load resistance

* Corresponding author: ahlam.ali@coeng.uobaghdad.edu.iq

http://dx.doi.org/10.28991/CEJ-2024-010-02-017

compared to conventional reinforced concrete columns [6]. Depending on the requirements for structural stiffness, strength, and ductility, various sectional shapes, such as H-sections, cruciform sections, twin or embedded sections, and tube sections, can be used in the CES columns [7]. The configuration of the encased steel section has a clear impact on the confining effect. Columns with a tube-shaped steel section provide better confinement, resulting in increased ductility and ultimate axial capacity of the columns [8, 9]. However, the compressive strength of concrete has increased, resulting in a higher load-carrying capacity but reduced ductility in encased composite columns [9].

In the second method, the full use of the properties of steel and concrete is achieved by using concrete-infilled steel tube columns (CFST). CFST sections, which are constructed from produced steel tube sections and concrete filling, have been widely used as a vertical bearing component. The main advantages offered by CFST include increased strength, ductility, significant cost savings, fire resistance, and quick installation due to the fact that the CFST column does not require the use of a reinforced cage or formwork [10–14]. The stability of the steel tube is enhanced by the concrete inside it. Furthermore, the steel tube effectively provides lateral confinement for the concrete. The confinement of steel tubes can increase normal and high-strength concrete's strength and ductility [15–18]. A few stirrups can be used in concrete-filled steel tube columns because the steel tube confines the concrete in a triaxial state [14]. In general, the strength of circular steel tube (CFST) columns is influenced by various factors. The thickness of the steel tube and the presence of longitudinal and hoop reinforcement tend to increase the ultimate strength, while the slenderness ratio has the opposite effect. Compared to other sectional shapes, circular steel tube columns tend to have a higher axial load and ductility [20]. Moreover, the bearing capacity of the CFST columns can be enhanced by increasing the compressive strength of the concrete [21]. To further increase the ultimate strength of CFST columns, various approaches can be taken. For instance, self-compacting concrete made with fly ash and silica fume [22], fiber-reinforced concrete [23], and micro-steel fiber concrete [24] have been found effective. Micro-steel fiber concrete has the added benefit of improving ductility and delaying local buckling of the column [24].

In the third method of reinforcement for columns, steel tubes of small diameters can replace longitudinal steel bars in normal reinforced concrete RC columns. For the same cross-sectional area, the circular steel tubes of small diameters achieve a higher second-moment area and radius of gyration than the steel bars. For that, the reinforcement of concrete columns in this method gives a higher stiffness and critical buckling load than the traditional reinforcement for concrete columns. The yield, ultimate strength, and ductility of the concrete columns under compression load can all be improved by filling these tubes with concrete [25, 26]. This is due to the concrete infill steel tube's ability to postpone local buckling and change the tube wall’s failure from an inward to an outward direction [27]. In their study, Hadi et al. [28] examined the behavior of columns that were reinforced with steel tubes under compression load. The researchers observed that the ductility of these columns improved significantly and that their ultimate strength was comparable to that of columns that were reinforced with traditional reinforcement. This was despite the fact that the yield tensile strength of steel bars is typically higher than that of steel tubes.

Because of all of the above, few studies have yet been conducted on this method of reinforcement. The steel tube with a small diameter infilled with cementitious grouting materials used as longitudinal reinforcement for columns may enhance the axial compression strength and the ductility of the column due to the confinement offered by the infill grouting material inside the steel tubes. For that, a new concept and parameters were used in this study to cover this method of reinforcement extensively. Also, this study treated the problem of using plain steel tubes in concrete column reinforcement because of the slip of the tubes in concrete.

The objective of the present study is to carry out an experimental and numerical investigation to assess the ultimate capacity of columns with tubes infilled with cementitious grouting material reinforcement. The first section of the study will involve experimental work to determine the impact of reinforcement type, spiral pitch, and slenderness ratio on ultimate load capacity, axial deformation, axial strain in longitudinal reinforcement, and failure mechanism. For verification of the predicted results, an analytical finite element model will be developed using ABAQUS software.

2. Experimental Program

2.1. Specimens Design

Twelve mid-scale circular column specimens were categorized into two groups, short and long concrete columns. All specimens have a diameter of 170 mm and two different heights of 750 and 1750 mm. The height-to-diameter (H/D) ratio for the first group (six short columns) is equal to 4.4 (i.e., greater than the ACI318-19 code limitation [29], which stated that member with a ratio of H/D less than or equal to 3 used primarily to support axial compressive load categorizes as a pedestal), while the slenderness ratio ($k\ l_u/r$) for the second group (six long columns) is equal to 41 (i.e., higher than the ACI318-19 code limitation, which stated that the slenderness effects can be neglected for columns braced against sidesway if ($k\ l_u/r \leq 34 + 12(M_1/M_2)$). The specimens were designed and tested under a uniaxial compression load. All column specimens were reinforced transversally with spiral reinforcement $\emptyset 6\ mm$ with spiral pitches of 50 or 75 mm. The pitch was chosen to satisfy the ACI requirements [29]. In each group, two specimens were reinforced with six longitudinal steel bars of $\emptyset 16$ mm, which are considered reference specimens. The other two

specimens were reinforced with six longitudinal steel tubes with an outer diameter of 16 mm (the gross cross-sectional area of the infilled cementitious grouting material steel tube is the same as the conventional steel bar area). The remaining two specimens were reinforced with six longitudinal steel tubes with an outer diameter of 25.4 mm (in which the wall cross-sectional area of the steel tube is the same as the steel bar area). The details of tested column specimens and reinforcement are shown in Table 1 and Figure 1.

Table 1. Reinforcement details of tested specimens

Group No.	Specimen ID	Specimen length (mm)	Diameter of steel bar or steel tube (mm)	Wall thickness of steel tube (mm)	Longitudinal reinforcement ratio (%)	Spiral pitch (mm)	Transverse reinforcement ratio (%)
Group 1	S-SB16-P50	750	16	-	5.31	50	1.74
	S-SB16-P75					75	1.16
	S-ST16-P50		16	1.3	1.59	50	1.74
	S-ST16-P75					75	1.16
	S-ST25.4-P50		25.4	2.8	5.31	50	1.74
	S-ST25.4-P75					75	1.16
Group 2	L-SB16-P50	1750	16	-	5.31	50	1.74
	L-SB16-P75					75	1.16
	L-ST16-P50		16	1.3	1.59	50	1.74
	L-ST16-P75					75	1.16
	L-ST25.4-P50		25.4	2.8	5.31	50	1.74
	L-ST25.4-P75					75	1.16

*In the specimen type, (S) refers to the short column, (L) refers to the long column, (SB) refers to the steel bar reinforcement, and (ST) refers to the steel tube reinforcement. The numbers (16) and (25.4) refer to the outer diameter of the steel bar and steel tube, respectively. The letter and number (P50) refer to a 50 mm pitch while (P75) refers to a 75 mm pitch.

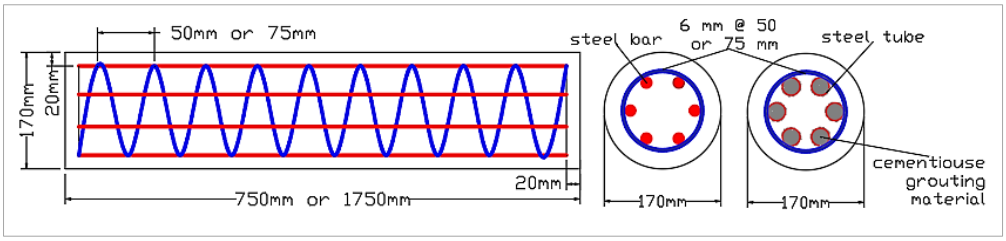

Figure 1. Cross-section and reinforcement details of column specimens

Because steel tubes of small diameters should be filled with concrete, cementitious grouting materials with high flowability were used to infill the tubes without any segregation. The steel tubes were filled with cementitious grouting material before installation in the specimens. After that, to prevent the slip of the plain steel tube in the concrete, the surface of the steel tube was roughened using epoxy and sand. Epoxy resin was utilized as the adhesive for this purpose. Before coating, the steel tubes were cleaned with sandpaper to remove the rust from their surfaces. The coating was applied to the surface of each steel tube with a paintbrush.

2.2. Material Properties

A target design cubic strength of 30 MPa at 28 days of age was used to cast all specimens using normal-strength concrete. Cementitious grouting material with a high compressive strength was used to infill all steel tubes, where the average compressive strength of 50 × 50 × 50 mm cube's dimensions at 28 days age and at the time of testing was 78.2 MPa and 83.3 MPa, respectively. The mechanical properties of steel bars and tubes are tabulated in Table 2.

Table 2. Mechanical properties of steel bar and steel tube reinforcement

Type of steel	Nominal outer diameter (mm)	Actual Area (mm^2)	Yield strength (MPa)	Ultimate strength (MPa)
Steel bars	6	26.42	489	624
	16	197	428	542
Steel tubes	25.4	198.8	316	413
	16	60.03	322	414

2.3. Test Setup and Instrumentation

All reinforced column specimens were tested in a 200 T capacity hydraulic testing rig under uniaxial compression load (Figure 2). Two loading end caps were designed and fabricated to achieve the pin-pin end supports (Figure 3). The two ends of the RC specimens were strengthened by one layer of carbon fiber reinforced polymer (CFRP) sheet of 100 mm width for short columns and 150 mm width for the long columns, and an overlap of 100 mm to prevent local crushing failure during the axial compression tests. All specimens had four strain gauges connected at the mid-height section, two for measuring the axial strains in the concrete and the other two for measuring the axial strains in the two opposing longitudinal reinforcements (bars or tubes). The axial displacement of the column specimens was measured with linear variable differential transformers (LVDT).

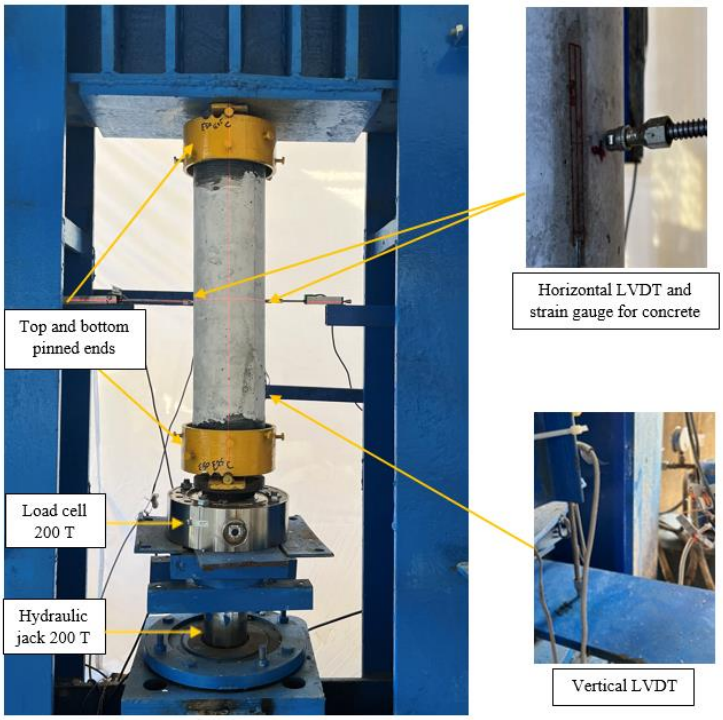

Figure 2. Test setup and instrumentation

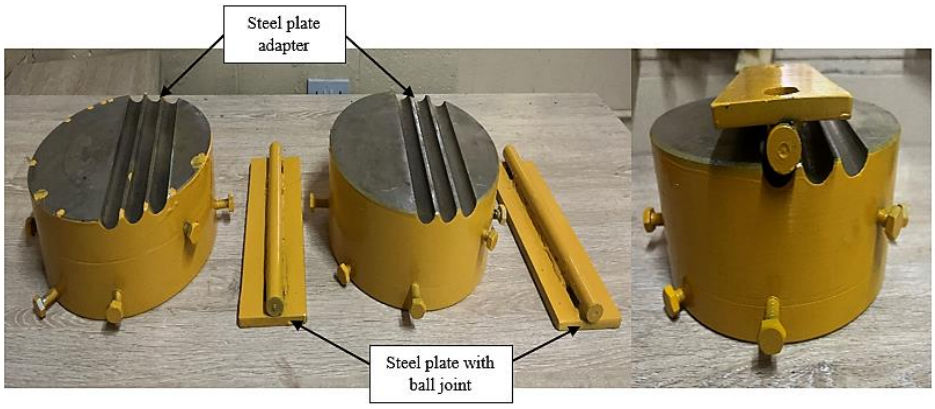

Figure 3. Loading caps

3. Finite Element Modeling

3.1. Material Constitutive Relationships

Three-dimensional nonlinear finite element analyses were performed using the ABAQUS Commercial software package [30] for simulations of RC columns. In this study, the concrete damaged plasticity CDP model included in mentioned software is chosen to simulate the inelastic behavior of concrete and cementitious grouting material [31].

Constitutive models for steel and concrete are needed to carry out the numerical analysis. Seanz constitutive model [32] for the uniaxial compressive stress-strain of concrete was adopted (Figure 4).

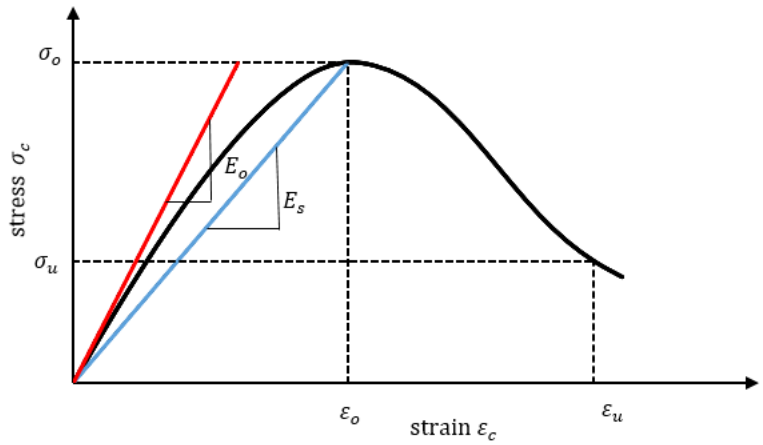

Figure 4. Uniaxial stress-strain model for concrete

$$\sigma_c = \frac{E_o \varepsilon_c}{1+\left(R+\frac{E_o}{E_s}-2\right)\frac{\varepsilon_c}{\varepsilon_o}-(2R-1)\left(\frac{\varepsilon_c}{\varepsilon_o}\right)^2+R\left(\frac{\varepsilon_c}{\varepsilon_o}\right)^3} \quad (1)$$

in which:

$$R = \frac{E_o(\frac{\sigma_o}{\sigma_u}-1)}{E_s(\frac{\varepsilon_u}{\varepsilon_o}-1)^2} - \frac{\varepsilon_o}{\varepsilon_u} \quad (2)$$

$$E_s = \frac{\sigma_o}{\varepsilon_o} \quad (3)$$

where E_o is the initial modulus of elasticity of concrete; and σ_c and ε_c are the concrete compressive stress and strain; σ_o and ε_o are the peak compressive stress of concrete and its corresponding strain; Two assumptions which were proposed by Elwi & Murray [32] were adopted in this study including $\sigma_o/\sigma_u = 4$ and $\varepsilon_u/\varepsilon_o = 4$.

A stress-strain model of concrete confined by circular steel tubes can be employed for FE modelling to model the cementitious grouting material inside the steel tubes. The model adopted by Tao et al. [33] was used in this study (Figure 5). A three-stage model is proposed to represent the strain hardening/softening of concrete confined by circular steel tubes. In the initial stage (from point O to point A), see Figure 5), the following model is used:

$$\sigma_c = f_c' \frac{AX+BX^2}{1+(A-2)X+(B+1)X^2} \quad (4)$$

where $X = {\varepsilon_c}/{\varepsilon_{co}}$; $A = \frac{E_c\,\varepsilon_{co}}{f_c'}$; $B = \frac{(A-1)^2}{0.55} - 1$

$$\varepsilon_{co} = 0.00076 + \sqrt{(0.626\, f_c' - 4.33) \times 10^{-7}} \quad (5)$$

where σ_c, $\varepsilon_c$are stress and strain of concrete, f_c', ε_{co} are peak stress and strain of unconfined concrete, E_c: modulus of elasticity of concrete and ε_{CC} is the peak strain of confined concrete is determined by the following equation at point B (Figure 5):

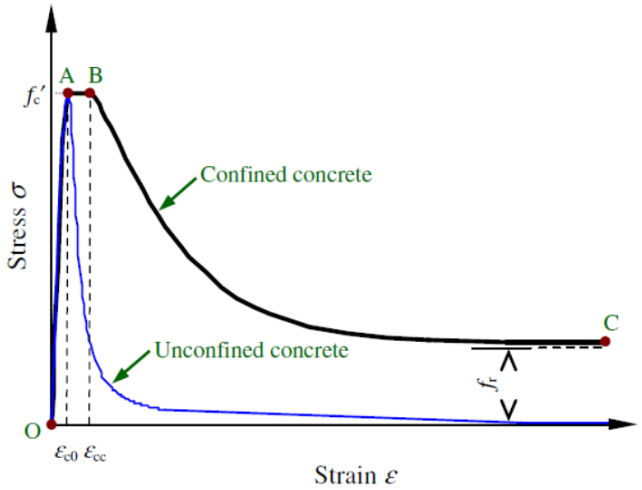

Figure 5. Uniaxial stress-strain model for grouting material

$$\varepsilon_{cc} = \varepsilon_{co}\, e^{k} \tag{6}$$

where;

$$k = (2.9224 - 0.00367\, f_c')\left(\frac{f_B}{f_c'}\right)^{0.3124+0.002\, f_c'} \tag{7}$$

f_B is the concrete's confining stress at point B, as indicated by the Equation 8.

$$f_B = \frac{(1+0.027 f_y)\, e^{-0.02\frac{D}{t}}}{1+1.6\, e^{-10}(f_c')^{4.8}} \tag{8}$$

Where $f_y$is the yield strength of the steel tube, D and t are the outer diameter and thickness of the steel tube. For the concrete model's descending part (BC), which is determined by:

$$\sigma = f_r + (f_c' - f_r)\exp[-\left(\frac{\varepsilon - \varepsilon_{cc}}{\alpha}\right)^{\beta}\ ; \qquad \varepsilon \geq \varepsilon_{cc} \tag{9}$$

where:

$$f_r = 0.7\left(1 - e^{-1.38\,\xi_c}\right); \qquad \leq 0.25\, f_c' \tag{10}$$

$$\alpha = 0.04 - \frac{0.036}{1+e^{6.08\xi_c - 3.49}} \tag{11}$$

$\beta = 1.2$ for circular CFST columns, and the confinement factor is $\xi_c = \frac{A_s f_y}{A_c\, f_c'}$.

The constitutive relationship for both longitudinal and transverse steel bars used an elastic perfectly plastic model. While the following stress-strain model was used for steel tubes [34], see Figure 6:

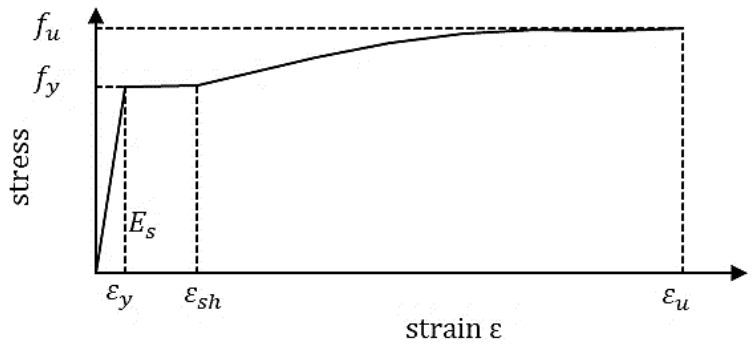

Figure 6. Stress-strain model for steel tube

$$f(\varepsilon) = \begin{cases} E\,\varepsilon\,; & \varepsilon < \varepsilon_y \\ f_y\ ; & \varepsilon_y < \varepsilon < \varepsilon_{sh} \\ f_y + (f_u - f_y)\left\{0.4\left(\frac{\varepsilon-\varepsilon_{sh}}{\varepsilon_u-\varepsilon_{sh}}\right) + \frac{2\left(\frac{\varepsilon-\varepsilon_{sh}}{\varepsilon_u-\varepsilon_{sh}}\right)}{\left[1+400\left(\frac{\varepsilon-\varepsilon_{sh}}{\varepsilon_u-\varepsilon_{sh}}\right)^5\right]^{\frac{1}{5}}}\right\}; & \varepsilon_{sh} < \varepsilon < \varepsilon_u \end{cases} \tag{12}$$

where f, ε are tensile stress and strain of steel; E is Young's modulus of steel; f_y, ε_y are yield stress and strain of steel; ε_{sh} is the hardening strain ($\varepsilon_{sh} = 0.1\frac{f_y}{f_u} - 0.055; 0.015 \leq \varepsilon_{sh} \leq 0.03$); f_u,is ultimate tensile stress of steel and ε_u is ultimate tensile strain of steel ($\varepsilon_u = 0.6\ (1 - \frac{f_y}{f_u})$).

3.2. Boundary Condition and Load Application

Pin-ended supports are the boundary conditions that were employed to simulate all column specimens. On one support, the displacements were constrained in all directions (x, y, and z) (hinge support). While the second support allowed for vertical displacements in the y-axis but restricted displacements in the x and z-axes. On the bottom surface of the column, the load was applied utilizing the displacement control approach with a 0.05 mm increment step.

3.3. Element Types and Mesh Configuration

The 3D concrete solid element, an 8-node linear brick element (C3D8R) with reduced integration, was adopted to model concrete, grouting material, and spirals. The steel bar was modelled using a standard 3-dimensional 2-node wire truss element (T3D2). While shell elements 4-node with the reduced integration S4R were used to model steel tubes. The embedded property was used to simulate the reinforcement (steel bar, steel tube with cementitious grouting material, and spiral reinforcement) in surrounding concrete. Except for the longitudinal steel bar reinforcement, which was discretized with a 40-mm mesh size, 20 mm mesh size was used for plain concrete, grout, steel tube, and spiral. This size of mesh was chosen to achieve the closest behavior to the experimental results.

4. Experimental Results and Verification

4.1. Load Displacement Response

The test results summary is tabulated in Table 3. Due to their different yielding stress, the steel tubes (ST16 and ST25.4) contribution to the axial capacity of the tested short and long columns (ST16-P50, ST16-P75, ST25.4-P50, and ST25.4-P75) was less for 26 and 25%, respectively, in comparison to the steel bars (SB16) contribution in the reference specimens (SB16-P50 and SB16-P75).

It is worth mentioning that in short and long columns reinforced with ST16, in which the steel tube area is 30% of the steel bar area, the maximum axial load of columns S-ST16-P50, S-ST16-P75, L-ST16-P50, and L-ST16-P75 attained 72, 71, 81 and 75% of the maximum load of the reference columns, respectively. This is a result of the significant confinement that the circular steel tubes provided for the cementitious grouting material, which increased the strength of the grout and increased the columns' ability to support more external load.

In short and long columns reinforced with ST25.4, in which the steel tube area is the same as the steel bar area, the maximum axial load of columns S-ST25.4-P50, S-ST25.4-P75, L-ST25.4-P50, and L-ST25.4-P75, exceeded the ultimate axial load of the reference column by 6, 5, 17 and 13%, respectively.

In a comparison test between two concepts for cementitious grouted steel-tube reinforcement, it was found that columns reinforced with 16mm outer diameter steel tubes achieved an ultimate strength of 68%, 68%, 69%, and 66% for S-ST16-P50, S-ST16-P75, L-ST16-P50, and L-ST16-P75 respectively, when compared to the ultimate strength of the specimens reinforced with 25.4mm outer diameter steel tubes, which were S-ST25.4-P50, S-ST25.4-P75-C, L-ST25.4-P50, and L-ST25.4-P75, respectively.

On the other hand, increasing the spiral pitch in column specimens from 50 mm to 75 mm led to a decrease in the maximum experimental axial load, as illustrated in Figure 7. Furthermore, from the test results, it was observed that the maximum experimental axial load of long columns was less than that for the short column with the same design parameters; this is associated with the slenderness ratio's effect on the axial capacity of the tested specimens, see Figure 8. Additionally, as the slenderness ratio increases, the experimental results show that the column's axial displacement increases (see Figure 9).

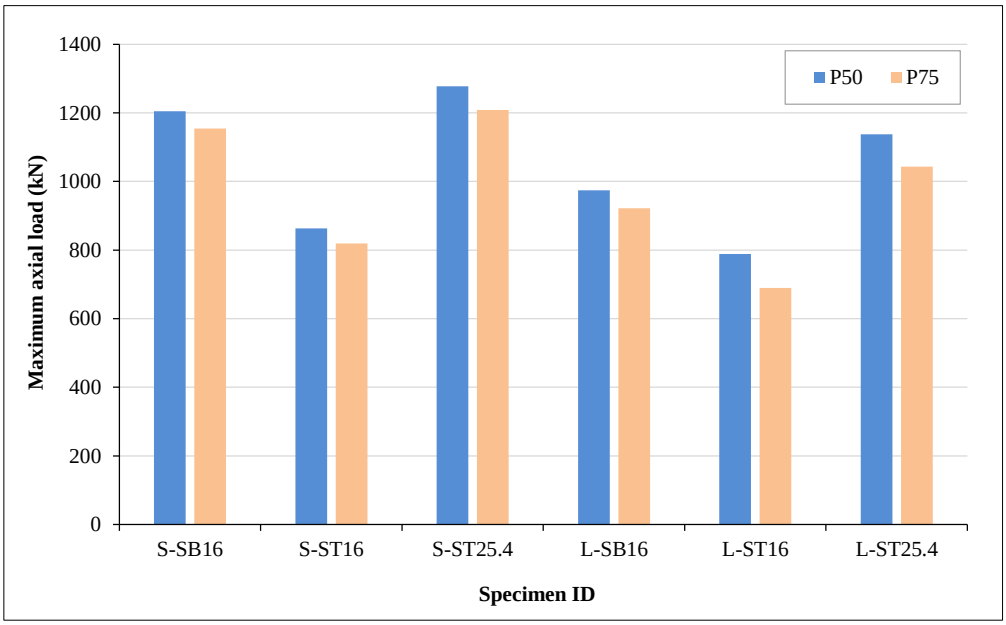

Figure 7. Effect of spiral pitch on the axial capacity of tested specimens

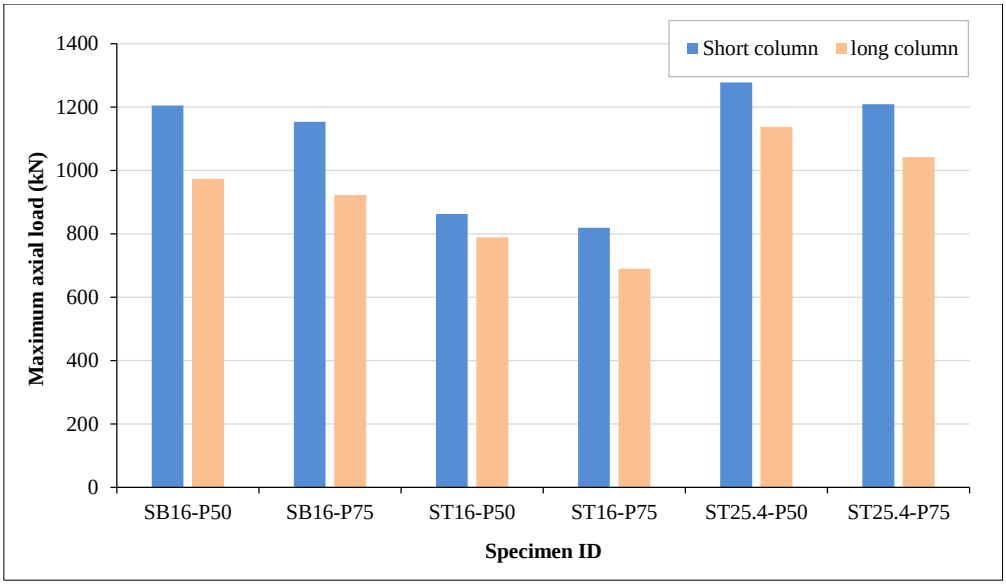

Figure 8. Effect of slenderness ratio on the axial capacity of tested specimens

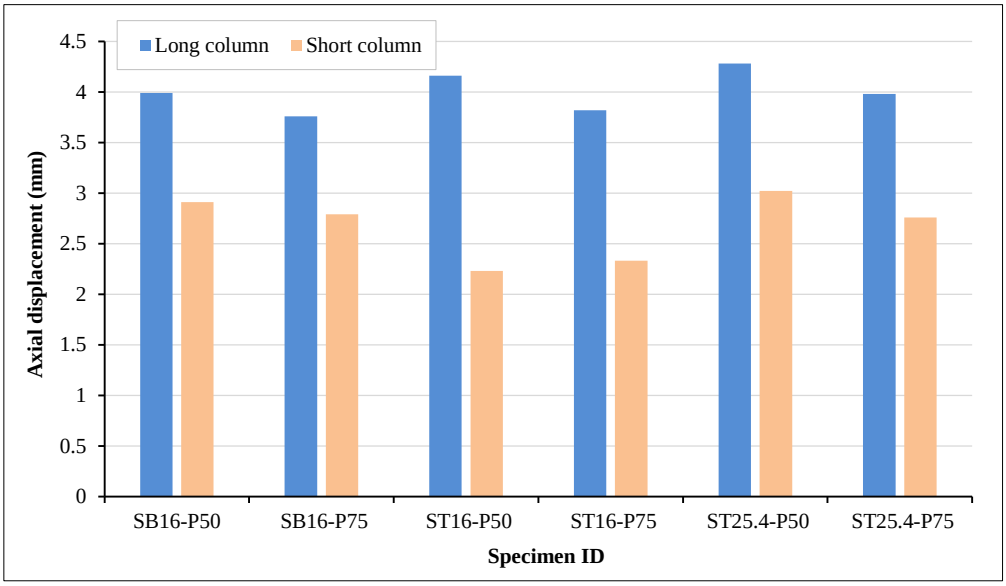

Figure 9. Effect of slenderness ratio on the axial displacement of tested specimens

Table 3 illustrates a comparison between the experimental and FE results for circular column specimens. Since the ratio (P_{exp}/P_{FEM}) is typically near to one, there is an acceptable agreement between numerically predicted values and those obtained experimentally. On the other hand, Figures 10 and 11 show the comparison between the FE axial load-axial displacement diagrams and those obtained experimentally. It can be observed from the figures that the stiffness of the FE curves for all tested specimens is higher than that of the experimental curves. This is because ABAQUS software assumes a perfect bond between the concrete and internal reinforcement, which is not the case in reality. However, the curves for the ascending part of the load-axial displacement curves demonstrate a reasonable convergence between the test and numerical results.

Table 3. Experimental and FE analysis results

Group No.	Specimen ID	Test Results		FE Results		P_{exp}/P_{FEM}
		P_{exp} (kN)	Δ_{exp} (mm)	P_{FEM} (kN)	Δ_{FEM} (mm)	
Group 1	S-SB16-P50	1205	2.91	1244	2.67	0.97
	S-SB16-P75	1154	2.79	1166	2.38	0.99
	S-ST16-P50	863	2.23	900	2.34	0.96
	S-ST16-P75	819	2.33	821	1.99	0.99
	S-ST25.4-P50	1278	3.02	1205	2.47	1.06
	S-ST25.4-P75	1209	2.76	1141	2.21	1.06

Group 2	L-SB16-P50	974	3.99	1064	3.86	0.92
	L-SB16-P75	922	3.76	977	3.52	0.94
	L-ST16-P50	789	4.16	817	3.98	0.97
	L-ST16-P75	690	3.82	729	3.4	0.95
	L-ST25.4-P50	1138	4.28	1140	4.2	0.99
	L-ST25.4-P75	1043	3.98	1071	3.78	0.97

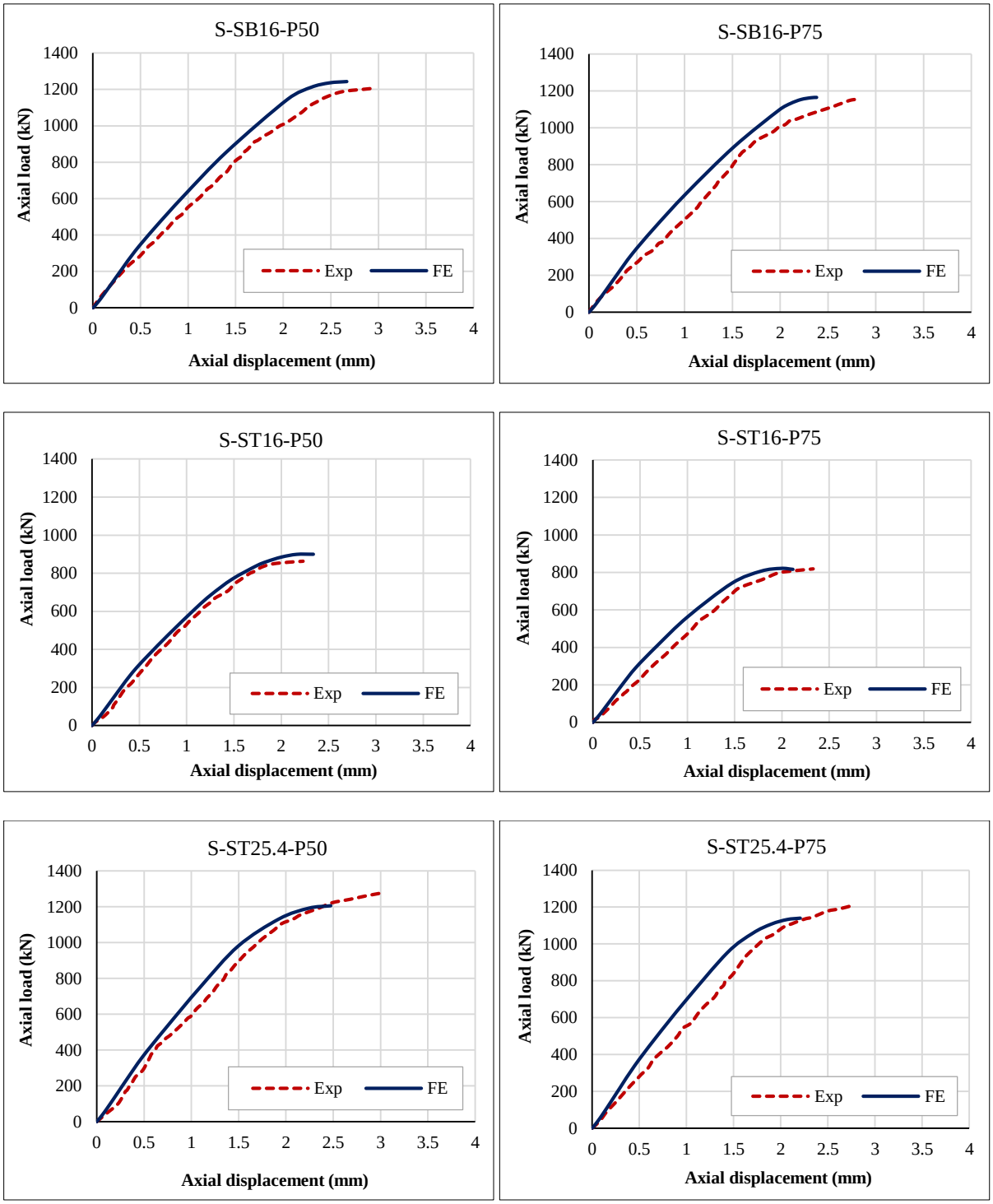

Figure 10. Load-axial displacement diagrams of short columns

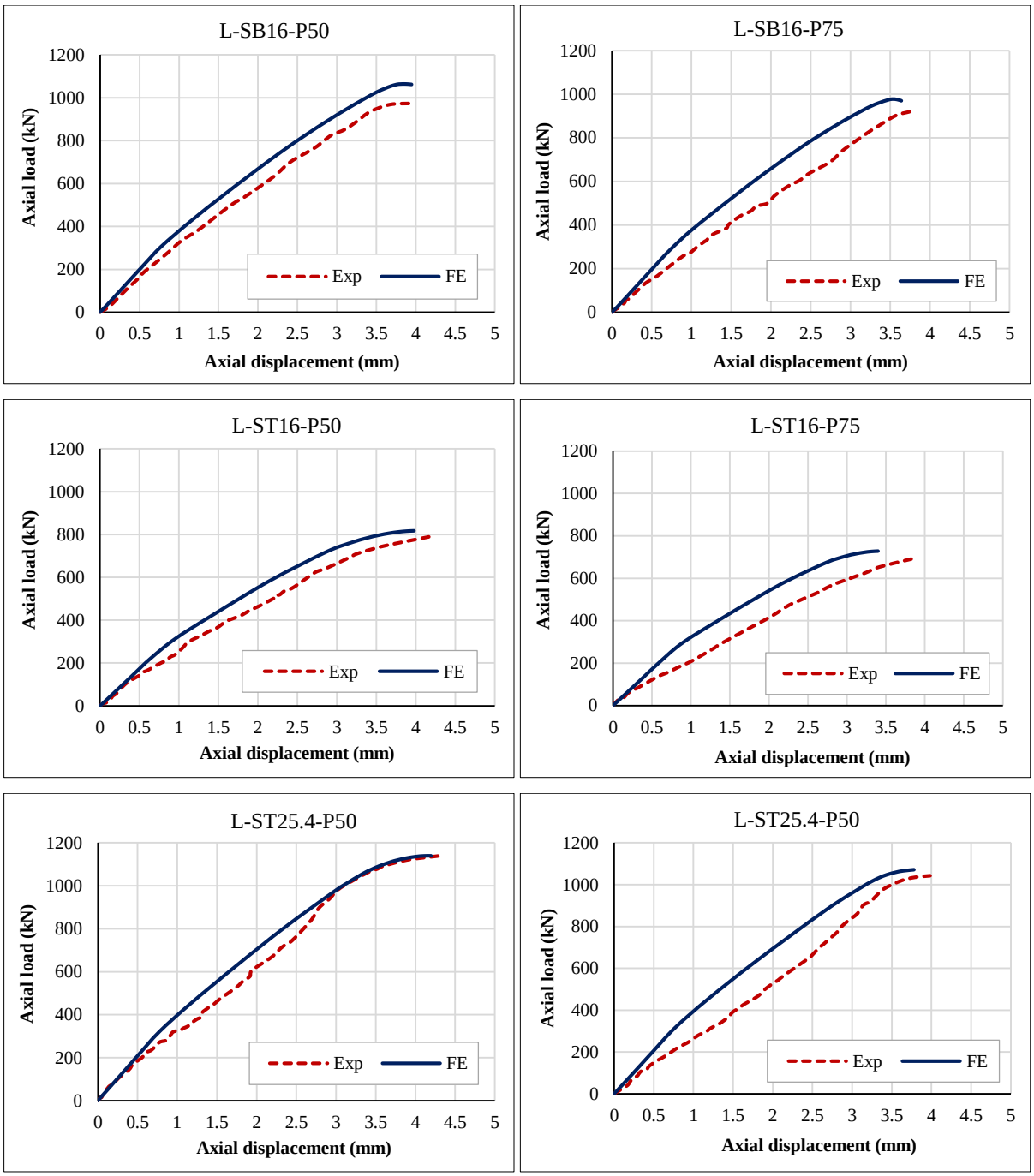

Figure 11. Load-axial displacement diagrams of long columns

4.2. Load-Strain Diagrams

The axial load versus axial strain according to the strain gauge readings at mid-height of concrete columns are illustrated in Figure 12 and Figure 13 for short and long columns, respectively. According to the data, only the specimens reinforced with steel bars (S-SB16-P50, S-SB16-P75, L-SB16-P50, and L-SB16-P75) showed an elastic behavior, since they did not reach the yield strain value. During this stage of performance, the load increased linearly as the strain increased. On the other hand, after the elastic stage, the axial load–strain curves of the specimens reinforced with steel tubes entered the yield stage, and the curve's slope started to decrease gradually, indicating that the steel tube began to yield. The strain in steel tubes of specimens S-ST16-P50, S-ST16-P75, S-ST25.4-P50, S-ST25.4-P75, L-ST16-P50, L-ST16-P75, L-ST25.4-P50, and L-ST25.4-P75 have attained the yield strain at an applied axial load of 0.86, 0.81, 0.8, 0.81, 0.84, 0.88, 0.83, and 0.86% from the maximum load. This is due to the fact that the yield strength of the steel bar is greater than the yield strength of the implemented steel tube. For this reason, the specimens with steel bars reinforcement failed by compression failure mode. At a certain applied load, specimens with the same design parameter showed higher strain as the slenderness ratio increased. This was due to reducing the depth of the compression zone of the section by increasing the secondary moment. On the other hand, Figures 12 and 13 illustrate that the FE outcomes of the load–axial concrete strain results matched well with the tested strain data.

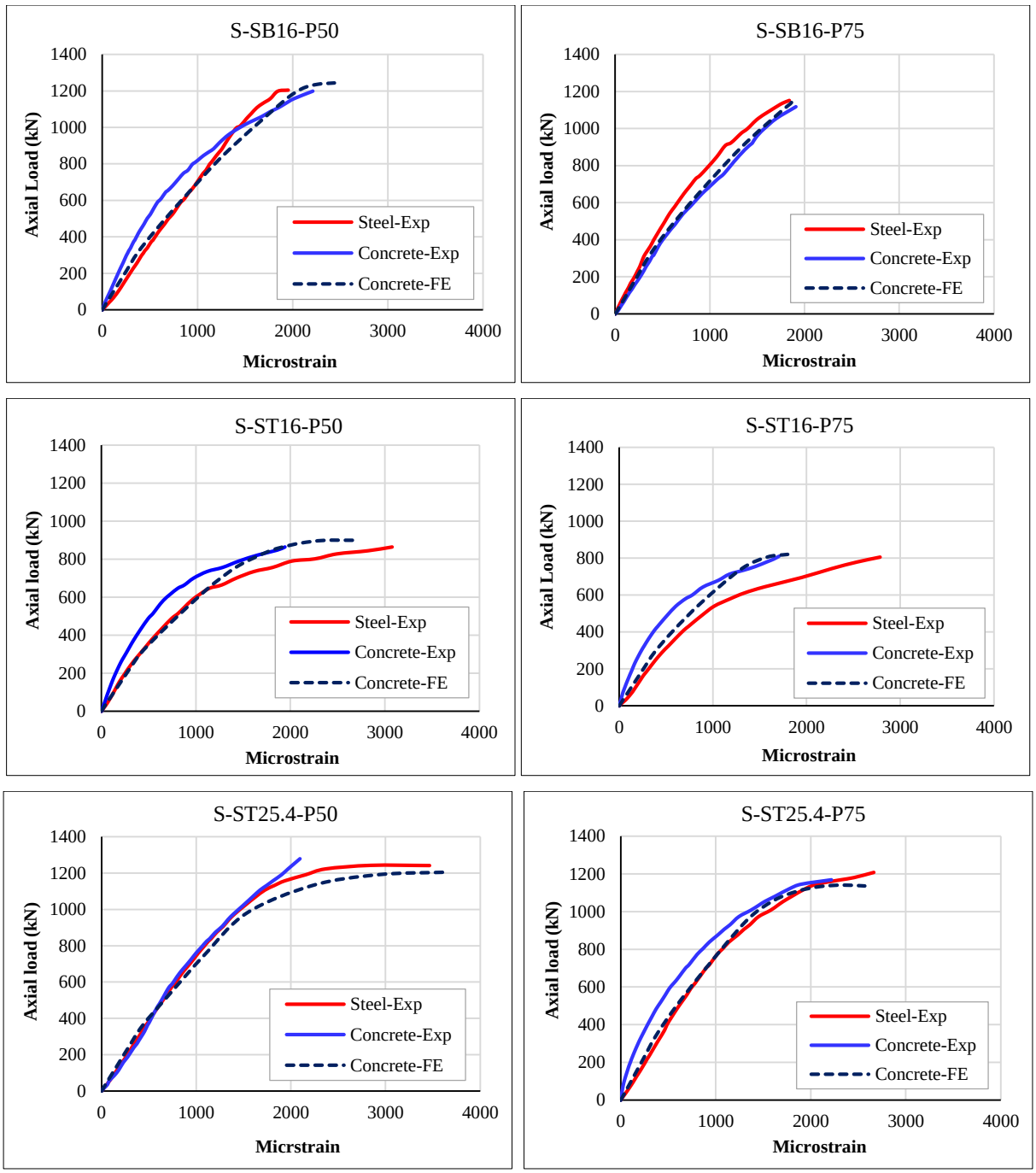

Figure 12. Axial load-axial strain diagrams for short columns

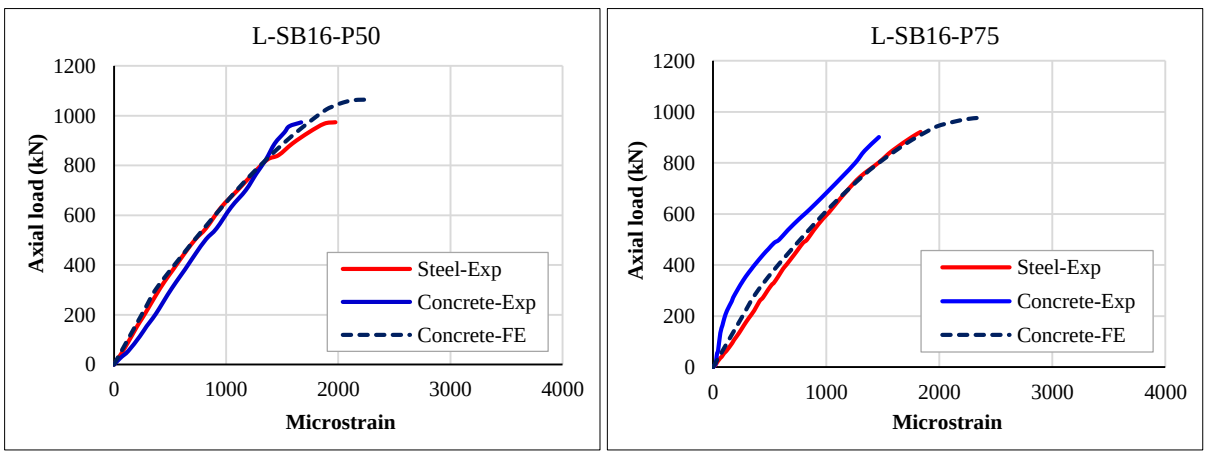

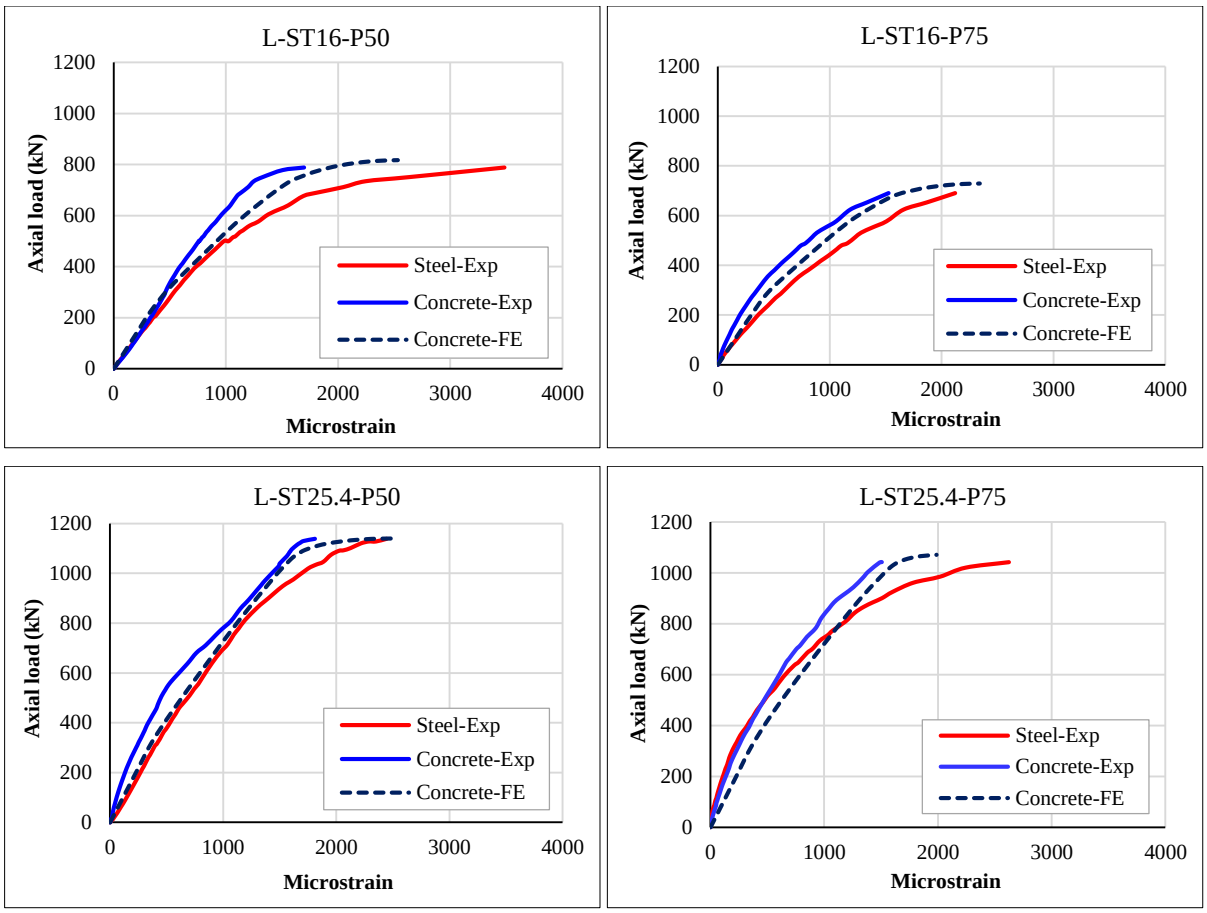

Figure 13. Axial load-axial strain diagrams for long columns

The failure mode of all experimental specimens was dominated by compression failure. Concrete cover spalling was observed at mid-height of almost all tested columns due to successive increases of applied loading, with no buckling observed in steel bars or tubes. The failure modes for all tested column specimens are shown in Figures 14 and 15 based on experimental and FE analysis findings. In all cases of short columns, the failure matched well with that seen in the experimental failure mode. In all columns, the failure occurred at the section located at mid-height of the tested specimens, except for specimens L-SB16-P50, L-SB16-P75, L-ST16-P50, and L-ST16-P75 specimens, the failure happened at the section located at the quarter length of the tested columns. A comparison of the failure zones of the experimental and the FE models illustrates the degree of agreement between the tested and the modeled specimens.

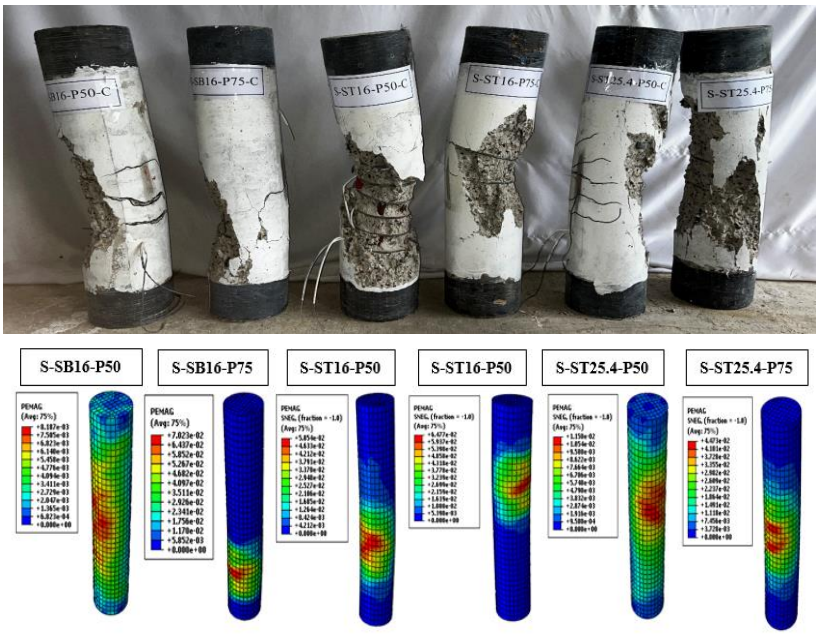

Figure 14. Failure mode of the experimental and FE analysis short columns

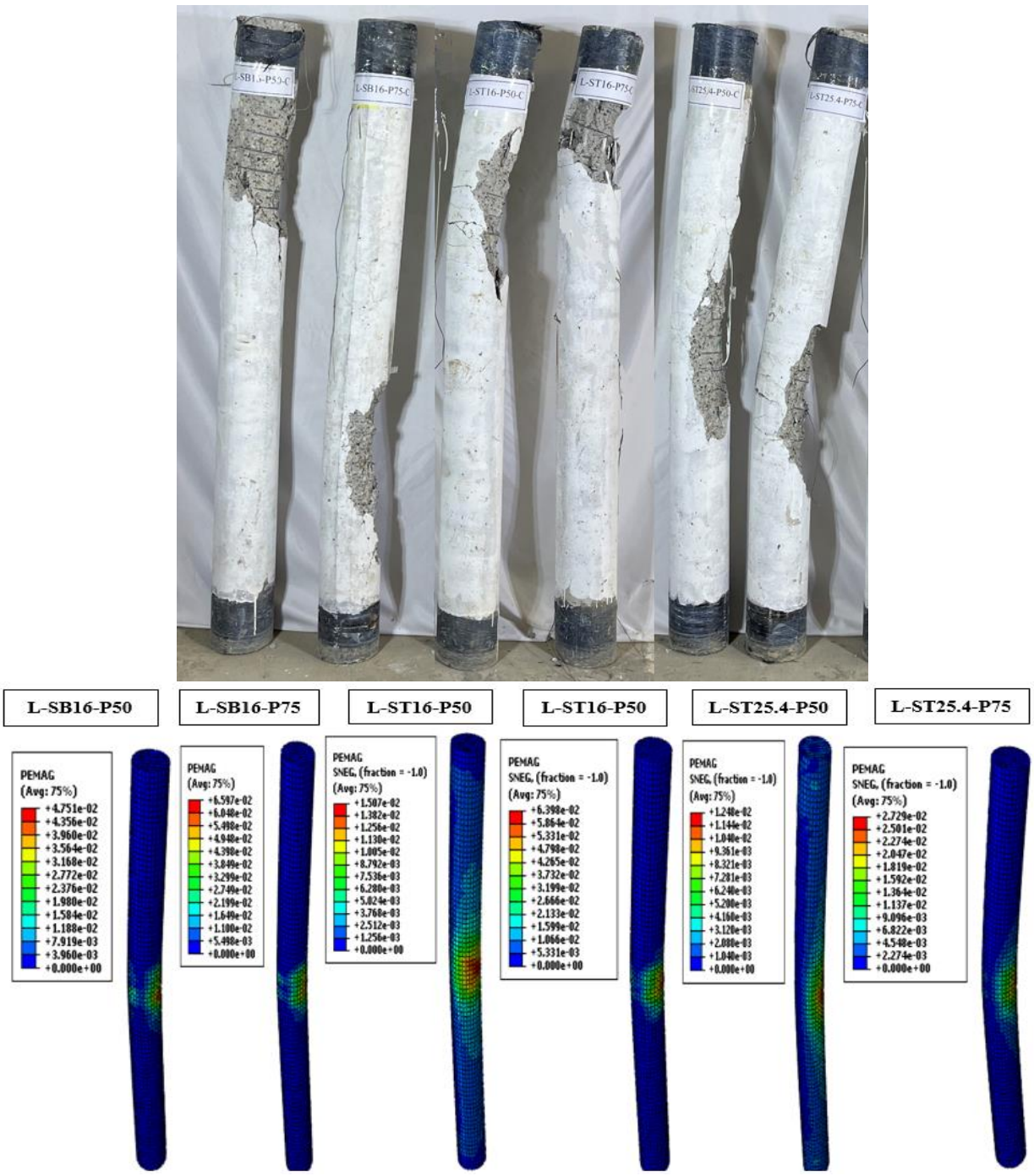

Figure 15. Failure mode of the experimental and FE analysis long columns

5. Conclusions

This article has presented a new form for longitudinally reinforced concrete columns. The columns with small-diameter cementiously grouted steel tube reinforcement under uniaxial compression load were investigated experimentally and numerically in this study. Based on the experimental results and FE analysis, the following conclusions are drawn:

- The load-carrying capacity of the columns with small-diameter steel tube reinforcement, having a steel cross-sectional area that is equivalent to the steel bars area used in reference specimens, increased compared to concrete columns reinforced with steel bars. While the loading capacity of concrete columns reinforced with steel tubes, having a cross-sectional area equal to not more than 30% of the steel bars area used in reference specimens, may be achieved at 81% of the load-carrying capacity of the reference columns.
- It is worth mentioning that in short and long columns reinforced with ST16, in which the steel tube area is 30% of the steel bar area, the maximum axial load of columns S-ST16-P50, S-ST16-P75, L-ST16-P50, and L-ST16-P75 attained 72, 71, 81, and 75% of the maximum load of the reference specimens, respectively.

- In short and long columns reinforced with S25.4, in which the steel tube area is the same as the steel bar area, the load carrying capacity of specimens S-ST25.4-P50, S-ST25.4-P75, L-ST25.4-P50, and L-ST25.4-P75 exceeded the ultimate axial load of the reference column by 6, 5, 17, and 13%, respectively.
- The maximum axial load decreased with the increase of spiral pitch from 50 to 75 mm in column specimens. Additionally, it was found that long columns with the same design parameters had lower maximum axial proposed loads than short columns; this is related to the slenderness ratio's effect on the loading capacity of the tested specimens.

The accuracy of the proposal model has been well confirmed by the close value of the axial compressive load, axial strain, and failure mode obtained from the FEM analysis as compared with the experimental results.

6. Declarations

6.1. Author Contributions

Conceptualization, A.A.A. and N.O.; methodology, A.A.A. and N.O.; software, A.A.A.; validation, A.A.A.; formal analysis, A.A.A. and N.O.; investigation, A.A.A. and N.O.; resources, A.A.A. and N.O.; data curation, A.A.A.; writing—original draft preparation, A.A.A.; writing—review and editing, N.O.; visualization, A.A.A.; supervision, N.O.; project administration, A.A.A.; funding acquisition, A.A.A. All authors have read and agreed to the published version of the manuscript.

6.2. Data Availability Statement

The data presented in this study are available on request from the corresponding author.

6.3. Funding

The authors received no financial support for the research, authorship, and/or publication of this article.

6.4. Conflicts of Interest

The authors declare no conflict of interest.

7. References

[1] Sakino, K., Nakahara, H., Morino, S., & Nishiyama, I. (2004). Behavior of Centrally Loaded Concrete-Filled Steel-Tube Short Columns. Journal of Structural Engineering, 130(2), 180–188. doi:10.1061/(asce)0733-9445(2004)130:2(180).

[2] Giakoumelis, G., & Lam, D. (2004). Axial capacity of circular concrete-filled tube columns. Journal of Constructional Steel Research, 60(7), 1049–1068. doi:10.1016/j.jcsr.2003.10.001.

[3] Choi, K.-K., & Xiao, Y. (2010). Analytical Model of Circular CFRP Confined Concrete-Filled Steel Tubular Columns under Axial Compression. Journal of Composites for Construction, 14(1), 125–133. doi:10.1061/(asce)cc.1943-5614.0000056.

[4] Lai, B. L., Zhang, M. Y., Zheng, X. F., Chen, Z. P., & Zheng, Y. Y. (2023). Experimental study on the axial compressive behaviour of steel reinforced concrete composite columns with stay-in-place ECC jacket. Journal of Building Engineering, 68, 106174. doi:10.1016/j.jobe.2023.106174.

[5] Mathew, S., & NI, N. (2021). Concrete Encased Steel Composite Columns: A Review. In Proceedings of the International Conference on Systems, Energy & Environment (ICSEE), Kerala, India. doi:10.2139/ssrn.3780548.

[6] Kartheek, T., & Das, T. V. (2020). 3D Modelling and analysis of encased steel-concrete composite column using Abaqus. Materials Today: Proceedings, 27, 1545–1554. doi:10.1016/j.matpr.2020.03.200.

[7] Liew, J. R., Xiong, M. X., & Lai, B. L. (2021). Design of Steel-Concrete Composite Structures Using High-Strength Materials. Woodhead Publishing, Sawston, United Kingdom. doi:10.1016/c2019-0-05474-x.

[8] Soliman, K. Z., Arafa, A. I., & Elrakib, T. M. (2013). Review of design codes of concrete encased steel short columns under axial compression. HBRC Journal, 9(2), 134–143. doi:10.1016/j.hbrcj.2013.02.002.

[9] Melesse, G., Jima, S., Asale, T., Moges, Y., & Kaske Kassa, H. (2023). Study on Mechanical Behavior of Fully Encased Composite Slender Columns with High-Strength Concrete Using FEM Simulation. Advances in Civil Engineering, 3581727. doi:10.1155/2023/3581727.

[10] Jegadesh, J. S. S., & Jayalekshmi, S. (2016). Using fibres and fly ash in concrete-filled steel tube columns. Proceedings of the Institution of Civil Engineers: Structures and Buildings, 169(10), 741–755. doi:10.1680/jstbu.15.00130.

[11] Aslani, F., Uy, B., Tao, Z., & Mashiri, F. (2015). Predicting the axial load capacity of high-strength concrete filled steel tubular columns. Steel and Composite Structures, 19(4), 967–993. doi:10.12989/scs.2015.19.4.967.

[12] Alshimmeri, A. J. H. (2016). Structural Behavior of Confined Concrete Filled Aluminum Tubular (CFT) Columns under Concentric Load. Journal of Engineering, 22(8), 125–139. doi:10.31026/j.eng.2016.08.08.

[13] Zhu, A., Zhang, X., Zhu, H., Zhu, J., & Lu, Y. (2017). Experimental study of concrete filled cold-formed steel tubular stub columns. Journal of Constructional Steel Research, 134, 17–27. doi:10.1016/j.jcsr.2017.03.003.

[14] Hassooni, A. N., & Al-Zaidee, S. R. (2022). Rehabilitation of Composite Column Subjected to Axial Load. Civil Engineering Journal (Iran), 8(3), 595–611. doi:10.28991/CEJ-2022-08-03-013.

[15] Elremaily, A., & Azizinamini, A. (2002). Behavior and strength of circular concrete-filled tube columns. Journal of Constructional Steel Research, 58(12), 1567–1591. doi:10.1016/S0143-974X(02)00005-6.

[16] Lahlou, K., Lachemi, M., & Aïtcin, P.-C. (1999). Confined High-Strength Concrete under Dynamic Compressive Loading. Journal of Structural Engineering, 125(10), 1100–1108. doi:10.1061/(asce)0733-9445(1999)125:10(1100).

[17] Hassooni, A. N., & Al Zaidee, S. R. (2022). Behavior and Strength of Composite Columns under the Impact of Uniaxial Compression Loading. Engineering, Technology and Applied Science Research, 12(4), 8843–8849. doi:10.48084/etasr.4753.

[18] Abadel, A. A. (2023). Structural Performance of Strengthening of High-Performance Geopolymer Concrete Columns Utilizing Different Confinement Materials: Experimental and Numerical Study. Buildings, 13(7), 1709. doi:10.3390/buildings13071709.

[19] Wang, X., Liu, J., & Zhang, S. (2015). Behavior of short circular tubed-reinforced-concrete columns subjected to eccentric compression. Engineering Structures, 105, 77–86. doi:10.1016/j.engstruct.2015.10.001.

[20] Hossain, K. M. A., Chu, K., & Anwar, M. S. (2021). Axial load behavior of ultrahigh strength concrete-filled steel tube columns of various geometric and reinforcement configurations. Infrastructures, 6(5), 66. doi:10.3390/infrastructures6050066.

[21] Ilanthalir, A., Jerlin Regin, J., & Maheswaran, J. (2020). Concrete-filled steel tube columns of different cross-sectional shapes under axial compression: A review. IOP Conference Series: Materials Science and Engineering, 983(1), 12007. doi:10.1088/1757-899X/983/1/012007.

[22] Mustapha, F. A., Sulaiman, A., & Mohamed, R. N. (2021). Performance of fly ash and silica fume self-compacting concrete filled steel tube stub columns under axial compression. IOP Conference Series: Materials Science and Engineering, 1144, 012012. doi:10.1088/1757-899x/1144/1/012012.

[23] Ma, X., Bao, C., Wang, H., Cao, J., Cao, F., & Lim, K. S. (2023). Study on Axial Compression Properties of a New Type of Fiber-Reinforced Square Concrete-Filled Steel-Tube Composite Column. Arabian Journal for Science and Engineering, 48(10), 13415–13427. doi:10.1007/s13369-023-07817-6.

[24] Shah, S. M. I., & Ganesh, G. M. (2023). Micro-Steel Fiber-Reinforced Self-compacting Concrete-Filled Steel-Tube Columns Subjected to Axial Compression. International Journal of Steel Structures, 23(4), 1031–1045. doi:10.1007/s13296-023-00747-x.

[25] Alhussainy, F., Sheikh, M. N., & Hadi, M.N.S. (2018). Axial Load-Axial Deformation Behaviour of SCC Columns Reinforced with Steel Tubes. Structures, 15, 259–269. doi:10.1016/j.istruc.2018.07.006.

[26] Alhussainy, F., Neaz Sheikh, M., & Hadi, M.N.S. (2019). P-m interactions of self-consolidating concrete columns reinforced with steel tubes. ACI Structural Journal, 116(3), 135–147. doi:10.14359/51714473.

[27] ANSI/AISC 360-10. (2010). Specification for structural steel buildings. American Institute of Steel Construction (AISC), Chicago, United States.

[28] Hadi, M.N.S., Alhussainy, F., & Sheikh, M. N. (2017). Behavior of Self-Compacting Concrete Columns Reinforced Longitudinally with Steel Tubes. Journal of Structural Engineering, 143(6), 4017024. doi:10.1061/(asce)st.1943-541x.0001752.

[29] ACI 318-19. (2019). Building code requirements for structural concrete and commentary. American Concrete Institute (ACI), Michigan, United States.

[30] ABAQUS version 6.14. (2019). Dassault Systemes Simulia, Johnston, United States.

[31] ABAQUS. (2019). Analysis User's Manual version 2019. Dassault Systemes Simulia, Johnston, United States.

[32] Elwi, A. A., & Murray, D. W. (1979). a 3D Hypoelastic Concrete Constitutive Relationship. ASCE J Eng Mech Div, 105(4), 623–641. doi:10.1061/jmcea3.0002510.

[33] Tao, Z., Wang, Z. Bin, & Yu, Q. (2013). Finite element modelling of concrete-filled steel stub columns under axial compression. Journal of Constructional Steel Research, 89, 121–131. doi:10.1016/j.jcsr.2013.07.001.

[34] Yun, X., & Gardner, L. (2017). Stress-strain curves for hot-rolled steels. Journal of Constructional Steel Research, 133, 36–46. doi:10.1016/j.jcsr.2017.01.024.